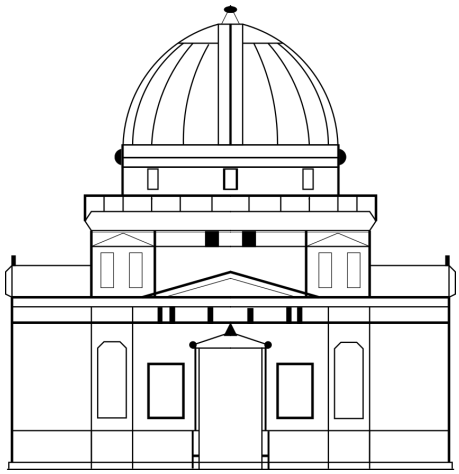

Strasbourg Astronomical Observatory

Numerical Simulation Project

Radiative transfer for the epoch of reionisation: Moment method, ATON-1D

Students:
Nicolas MAI
Samuel VALENTIN

Supervisor:
Pierre OCVIRK

Master of Astrophysics
2022-2023

Contents

1 Introduction

The reionisation era is a crucial period in the history of the Universe, marked by the transition from a largely neutral to a highly ionised state of the matter. This process is thought to have occurred approximately 300 million years after the Big Bang, when the first stars and galaxies formed and began to emit intense ultraviolet radiations. As this radiation interacted with the neutral hydrogen of the intergalactic medium, it ionised it, in other words stripped it off of its electrons. This reionisation process is believed to have had a significant impact on the evolution of the Universe, shaping the distribution of matter and the formation of structures such as galaxies and galaxy clusters. Despite its importance, the details of the reionisation era remain somewhat mysterious, and much of what we know about this period is based on indirect observations and theoretical models.

This project aims to create a 1D radiative transfer code that utilises the photon gas approach used in ATON. This code will be applied to various astrophysical scenarios, and even if only describing a 1D system, it will allow us to study the advancement of ionisation fronts in a neutral medium after the formation of stars in new born galaxies, which cannot be accurately modelled through analytical means. The main focus of this project is to investigate how the medium (in our case initially solely made of HI) impacts the propagation of radiation, slowing ionisation fronts, ultimately resulting in trapping those radiations into a finite volume. It is also important to recognise that the photon gas approach, while being a useful approximation for radiative transfer, does have its limitations.

This paper is articulated in three parts. The numerical methods and its implementation are described in Section 2 as well as different types sources. It includes the solution to the problem for the pure advective case (that is without taking into account any kind of possible photoionisation) and also in a chemical case, being more realistic and taking into account the photoionisation. Section 3 describes the results obtained and gives a physical interpretation. Then Section 4 introduces the concept of parallel computing and hints towards some ways our code could be parallelised.

2 Numerical methods

2.1 Basics

The numerical methods described in this section include two modules, performing the time evolution of a propagation front from a source emitting UV photons in 1D. The 1D computational domain is a series of n cells of width Δx disposed in a way that imposes boundary conditions. The inner properties of each cells such as the number density of photons, the flux or the pressure will have to be computed at each time steps, in order to follow the evolution of the photon propagation.

The first module aims to compute the displacement of the photons within the computational domain for a pure advective case. The second module introduces a coupling between the particles emitted by the source and the interstellar medium which we remind is here assumed to be initially purely made of neutral hydrogen.

2.2 Derivation of the equations

The method which we will be using is a moment-based method, meaning that we are going to describe the momentum of the radiative transfer equation while conserving the radiated energy and flux. We first remind what is the expression of the radiative transfer equation:

$$\frac{1}{c}\frac{\partial I_\nu}{\partial t} + \mathbf{n}\cdot\nabla I_\nu = -\kappa_\nu I_\nu + \eta_\nu \tag{1}$$

where I_ν is the specific intensity, κ_ν the absorption coefficient and η_ν the source function. In order to get to the equations we will use, we need to calculate the 0^{th} and 1^{st} moments of Eq.1. This will lead us to a system of two coupled equations. But let us first start with the 0^{th} order:

$$\frac{1}{c}\frac{\partial}{\partial t}\int I_\nu d\Omega + \int \nabla \underbrace{\cos(\theta)}_{(*)} I_\nu d\Omega = -\kappa_\nu \int I_\nu d\Omega + \eta_\nu \int d\Omega$$

where the infinitesimal solid angle $d\Omega = \sin(\theta)d\theta d\phi$ and the $(*)$ comes as the result of the dot product between the vectors $\mathbf{n}$ and ∇I_ν. The previous expression can be drastically simplified, using the results of the moments of the specific intensity we get:

$$\frac{\partial E_\nu}{\partial t} + \nabla \mathbf{F}_\nu = -\kappa_\nu c E_\nu + S_\nu \quad \Rightarrow \quad \frac{\partial N_\nu}{\partial t} + \nabla \mathbf{F}_\nu = -\kappa_\nu c N_\nu + S_\nu \tag{2}$$

the result has been obtained by dividing the first equation by the energy $E_\gamma = h\nu$ of a single photon of frequency ν. Hence, we introduce N_ν, the photon density. In a similar fashion, we can now perform the calculation for the 1^{st} order moment:

$$\frac{1}{c}\frac{\partial}{\partial t}\int I_\nu \cos(\theta) d\Omega + \int \nabla \cos^2(\theta) I_\nu d\Omega = -\kappa_\nu \int I_\nu \cos(\theta) d\Omega + \eta_\nu \int \cos(\theta) d\Omega$$

where we can realise that the last term is null because $\int \cos(\theta)\sin(\theta)d\theta d\phi = \pi \cos^2(\theta)\big|_{\theta=0}^{\theta=\pi} = 0$. As before, using the moments of the specific intensity we can get:

$$\frac{\partial \mathbf{F}_\nu}{\partial t} + c^2 \nabla \mathbf{P}_\nu = -\kappa_\nu c \mathbf{F}_\nu \tag{3}$$

The Eq.2 & 3 are not yet ready to be implemented into a numerical scheme because we lack the expression of their terms. In their article from 2008 about a radiative transfer numerical scheme, D.Aubert & R.Teyssier[1], explicitly determine those terms. We now present this set of equations with a quick explanation of the numerical scheme that they have developed:

$$\frac{\partial N_\gamma}{\partial t} + \nabla \mathbf{F}_\gamma = \underbrace{-n_{\text{H}_0} c \sigma_\gamma N_\gamma}_{(1)} + \underbrace{\dot{N}_\gamma^* + n_{\text{e}} n_{\text{H}_+}(\alpha_{\text{A}} - \alpha_{\text{B}})}_{(2)} \tag{4}$$

$$\frac{\partial \mathbf{F}_\gamma}{\partial t} + c^2 \nabla \mathbf{P}_\gamma = -n_{\text{H}_0} c \sigma_\gamma \mathbf{F}_\gamma \tag{5}$$

In Eq.4, the (1) corresponds to the absorption, in other words, this determines how far light of a particular wavelength will be able to travel through the neutral hydrogen medium before getting absorbed. We will consider a neutral hydrogen number density (n_{H_0}) of a few particles per cm^3 ($\in [3-6]$) and a cross section $\sigma_\gamma = 1.63 \times 10^{-18}\text{cm}^2$. In that same Eq.4, the (2) corresponds to the source term and can be sub-divided into two "sub-terms". The first one,

$\dot{N}_\gamma^*$, properly being the term accounting for the radiation coming from the sources (e.g.a star). The second "sub-term" accounts for the radiation coming from the recombination of H_+ that had previously been ionised. We can note that in order to maintain the charge conservation we need $n_e = n_{H_+}$ and $n_H = n_{H_0} + n_{H_+}$. Finally, α_A and α_B are recombination coefficients for H_+.

Assuming a radiation angular distribution which is axisymmetric around the flux vector $\mathbf{F}$, we can define the Eddington tensor (or stress tensor) $\mathbf{P}$ as a function of N with $\mathbf{P} = \mathbf{D}N$.

$$\mathbf{D} = \frac{1-\chi}{2}\mathbf{I} + \frac{3\chi - 1}{2}\mathbf{u} \otimes \mathbf{u} \quad \overset{1D}{\Longrightarrow} \quad \mathbf{D} = \chi \tag{6}$$

where χ is the Eddington factor, a scalar quantity. Defining the reduced flux $\mathbf{f}$ as

$$\mathbf{f} = \frac{\mathbf{F}}{cN} \tag{7}$$

Levermore[3], in his article from 1984 found an expression of χ depending on $\mathbf{f}$:

$$\chi = \frac{3 + 4|\mathbf{f}|^2}{5 + 2\sqrt{4 - 3|\mathbf{f}|^2}} \tag{8}$$

Having an expression for $\mathbf{P}$ as a function of N and $\mathbf{F}$ will come really handy in the resolution of our equations. Now that all the terms have been described, we can finally get into the details of the numerical implementation. The method used by D.Aubert & R.Teyssier[1] consists into decomposing the calculations of the terms of the equations in several steps.

2.3 Stellar source step

The first step is probably the most simple one and consists into "initialising" the number of photons in each of the Nb cells as well as the initial fluxes, pressures all being null. These initial conditions will obviously depend on the nature of the source we want to study and the state of the system when initialising the problem, however their time evolution will always be dictated by the following relation:

$$(N_\gamma)_i^{n+1} = (N_\gamma)_i^n + \dot{N}_\gamma^* \Delta t \tag{9}$$

where the index i designates the cell number and therefore runs from 0 to Nb-1. On the other hand, n designates the time step. In Section 3 we will present some results for different types of sources (pulse, continuous, double, packet) but for now let's describe how to compute this using a python script. The "method" we used was to work with lists of lists as shown on the figure below.

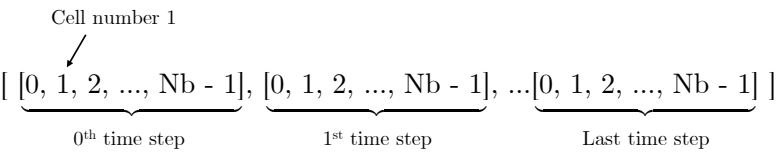

This method has the advantage of saving all the different quantities in all cells at any time step, therefore it allows us to freely use the resulting data for our results. However, this also means that the memory necessary for the whole simulation is high and can only be performed to some extents.

2.4 Transport step

For the second step we solve the advective equations, on one hand this physically means only taking into account the propagation of the radiation, and on the other hand it mathematically means equating to zero the left hand sides of Eq.4 & 5. Using the definition of the derivative and implementing it into an explicit scheme we get:

$$\frac{\partial N_\gamma}{\partial t} + \nabla \mathbf{F}_\gamma = 0 \quad \Rightarrow \quad \frac{(N_\gamma)_i^{n+1} - (N_\gamma)_i^n}{\Delta t} + \frac{(F_\gamma)_{i+1/2}^n - (F_\gamma)_{i-1/2}^n}{\Delta x} = 0 \tag{10}$$

$$\frac{\partial \mathbf{F}_\gamma}{\partial t} + c^2 \nabla \mathbf{P}_\gamma = 0 \quad \Rightarrow \quad \frac{(F_\gamma)_i^{n+1} - (F_\gamma)_i^n}{\Delta t} + c^2 \frac{(P_\gamma)_{i+1/2}^n - (P_\gamma)_{i-1/2}^n}{\Delta x} = 0 \tag{11}$$

where the $i \pm 1/2$ indices mean the value at the intercell. Using the GLF method described by M.González et al. in 2007[4], we can get an expression for the flux and the pressure at the intercell:

$$(F_{\mathrm{GLF}})_{i+1/2}^n = \frac{1}{2}(F_i^n + F_{i+1}^n) - \frac{c}{2}(N_{i+1}^n - N_i^n) \tag{12}$$

$$(P_{\mathrm{GLF}})_{i+1/2}^n = \frac{1}{2}(P_i^n + P_{i+1}^n) - \frac{c}{2}(F_{i+1}^n - F_i^n) \tag{13}$$

We can get the time evolution $(n+1)$ of $(N_\gamma)_i^{n+1}$ and $(F_\gamma)_i^{n+1}$ (in each i cell) by isolating them from respectively Eq.10 & 11. On the other hand we can get intercell evolution $(i+1/2)$ of $(F_{\mathrm{GLF}})_{i+1/2}^n$ and $(P_{\mathrm{GLF}})_{i+1/2}^n$ at a given time n from respectively Eq.12 & 13. With that we have all the elements that will allow us to make our numerical scheme that we now further explain.

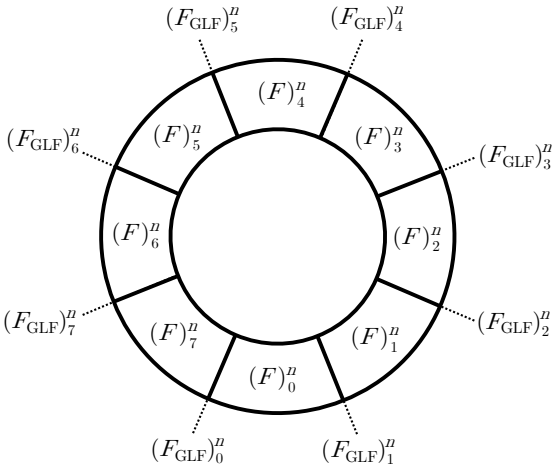

Figure 1: Schematics of our numerical scheme.

- The first step would be to consider the 0^{th} time iteration where the system has not evolved in any way yet. It is therefore reasonable to assume that the fluxes and pressures are null while the number of particles in each cells is the one we have imposed via the initial conditions (e.g.pulse, continuous...). Hence, we have everything to calculate the two GLF and then the values of N, F and P.

- A first "complexity" is introduced by the boundary of the system, for instance located between $(F)_7^n$ and $(F)_0^{n+1}$ on Fig.1 (for clarity, we remind that after a full revolution, the n indices all change to $n+1$). Indeed, because of its periodicity, the GLF +1/2 of the last cell is shared with the -1/2 of the first cell. In the case of our example (see Fig.1), calculating $(F)_7^n$ would require a sort of fictive $(F_{\mathrm{GLF}})_8^n$, but because of our boundary condition, this one can be assumed to be $(F_{\mathrm{GLF}})_0^n$. Applying a similar treatment for N, we can get all the values for N, F and P at the first time iteration and then simply repeat the process.

- A similar problem occurs again at the boundary but this time for the determination of $(F_{\mathrm{GLF}})_0^{n+1}$, indeed, this one implies to know the fluxes in the two neighbouring cells. In that case, we have to implement in the code that the cell preceding the $(F_{\mathrm{GLF}})_0^{n+1}$ for any $n > 1$ will be $(F)_7^{n-1}$ (again the seven is here arbitrary but more generally corresponds to the last cell of the system).

2.5 Thermochemical step

The previous treatment of the front propagation did not take into account the possible interaction of the photons with the surrounding interstellar medium. This coupling will now be considered and by taking into account such effects, it is expected that the propagation front will decrease in intensity as it travels through the neutral gas due to the absorption of photon by the medium. This treatment will be discussed and implemented in this section assuming the hydrogen gas as isothermal.

One effect responsible of such phenomenon is the photoionisation of the neutral hydrogen atom, driven by the following reaction:

$$H + \nu \longrightarrow H^+ + e^- \tag{14}$$

In the Universe, it happens in hydrogen clouds which absorb the incoming UV photons opacifying the medium. This neutral gas acts as a "shield" and makes it harder for the photons to freely travel without being absorbed on their way. Four main phenomena can be accounted for this opacification, bound-bound transitions, bound-free (photoionisation), free-free and Thomson scattering. In general, in neutral regimes where the electrons are bound to their atoms, the cross section of the photoionisation is high compared to the Thomson scattering while it becomes smaller in ionised medium at the expense of the latter. However, it means that if we only take into account photoionisation, once the hydrogen has been ionised in a given region, it becomes transparent to the photons which can freely propagate.

The module for the radiation and ionisation coupling that we have implemented for the photoionisation is discussed by D.Aubert & R.Teyssier[1]. First we have to calculate the hydrogen fraction x in each cells at every time step. To do so, we systematically have to compute a third order polynomial, for which, one of the roots is the ionisation fraction in a given cell for the time iteration $n+1$.

$$Q_3(X) = mX^3 + nX^2 + pX + q \tag{15}$$

with the different coefficients of this equation given by:

$$m = (\alpha_B + \beta)\rho^2 \Delta t \tag{16}$$

$$n = \rho - (\alpha + \beta)\frac{\rho}{\sigma_\gamma c} - \alpha_B \rho^2 \Delta t - 2\beta\rho^2 \Delta t \tag{17}$$

$$p = -\rho(1+x) - N'_\gamma - \frac{1}{\sigma_\gamma c \Delta t} + \frac{\beta\rho}{\sigma_\gamma c} + \beta\rho^2 \Delta t \tag{18}$$

$$q = N'_\gamma \rho x + \frac{x}{\sigma_\gamma c \Delta t} \tag{19}$$

where α, α_B and β are functions defining the recombination and the collisional ionisation rates[2] and all strongly depending on the temperature, ρ is the initial hydrogen density, x the ionisation fraction, N'_γ the density number of photons and σ_γ the photoionisation cross section.

As stated above, the hydrogen fraction is recovered by computing the different solutions of this third order equation. In our implementation we have used the numpy function `np.roots`, which returns the solution of a polynomial[1]. As a result, we can deduce the value of the ionised fraction at time $n+1$ in cell i: $X = x_i^{n+1}$. Now that this value has been computed, we can include it in the explicit advection equations (describing photons propagation without any neutral hydrogen). The new advection equations for the number density of photons and the flux read:

$$N_\gamma^{n+1} = N'_\gamma + \beta\rho^2(1-X)X\Delta t - \alpha_B \rho^2 X^2 \Delta t - \rho(X - x) \tag{20}$$

$$F_\gamma^{n+1} = \frac{F'_\gamma}{1 + c\sigma_\gamma \rho \Delta t(1-X)} \tag{21}$$

From this new set of equations, it is possible to simulate the photons propagation through a neutral hydrogen gas cloud considering photoionisation effects.

2.6 Temperature coupling

For now and for the entirety of this report we are only going to consider a system of constant temperature. However, as we may expect it from a physical intuition, temperatures do change in each cells as a function of time because of effects such as the excitation due to the photoionisation... This small sub-section aims to explain how to account for this phenomena but we won't be able to show any results because we couldn't get satisfying solutions.

In principle, knowing $(x)^{n+1}$, the ionisation fraction at a time $t + \Delta t$, we can estimate the value of $(T)_\gamma^{n+1}$, that is the evolution of the temperature[2]. This gives us:

$$(T)^{n+1} = \frac{2(\mathcal{H} - \mathcal{L})\Delta t + T^n B}{B + 2\Delta t A} \quad \text{with} \quad \begin{cases} A = \frac{3}{2}\rho(1+X)k_B(X-x)/\Delta t \\ B = 3\rho(1+X)k_B \end{cases} \tag{22}$$

where the two main unknowns here are $\mathcal{H}$, the heating rate and $\mathcal{L}$ the cooling rate. The expression for the heating rate can be recovered by ourselves quite easily simply by stating as

[1] We can note that another possible method that we have not here implemented, could have been to compute the roots using the Newton-Raphson algorithm.

[2] Computationally speaking and based on how we've constructed our code, that means that we have to also create a list of temperatures presenting the same structure as the F, P or x.

a first approximation that it corresponds to the energy given to the electrons of the medium after each time step. This translates to:

$$\mathcal{H} = \underbrace{\rho \Delta x^3}_{(1)} \times \underbrace{(X - x)}_{(2)} \times \underbrace{(E_\gamma - 13.6)eV}_{(3)} \tag{23}$$

where (1) corresponds to the total number of particles in a cell, (2) to the fraction of atoms that has been ionised between a time t (for x) and $t + \Delta t$ (for X) and (3) the average energy given by a photon (of energy E_γ) to an electron and therefore translated into kinetic energy increasing the temperature. We can't recover the expression of the cooling rate $\mathcal{L}$ as easily, but it is computed using four different collisional cooling processes all given by Hui & Gnedin[2]. With all this, Eq.22 allows us to compute the temperature evolution in every cell.

3 Results

In this subsection we will only consider the case of the advective solution to the problem, that is without taking into account the thermochemistry. But let's first ponder about what should be our initial conditions.

3.1 Propagation

Indeed, we have to initialise our variables with values that will give us a result which physically makes sense. This constraint on the initial condition is given by what is called the current condition 'Cr'. It corresponds to the ratio between the distance travelled by light during a given time interval Δt and the length of a cell Δx. For any numerical scheme, we want this ratio to be inferior to 1. If it was not the case, it would mean that some information about our system between two following time iterations could jump over one or multiple cells. This mathematically translates to:

$$\mathrm{Cr} = \frac{c\Delta t}{\Delta x} < 1 \tag{24}$$

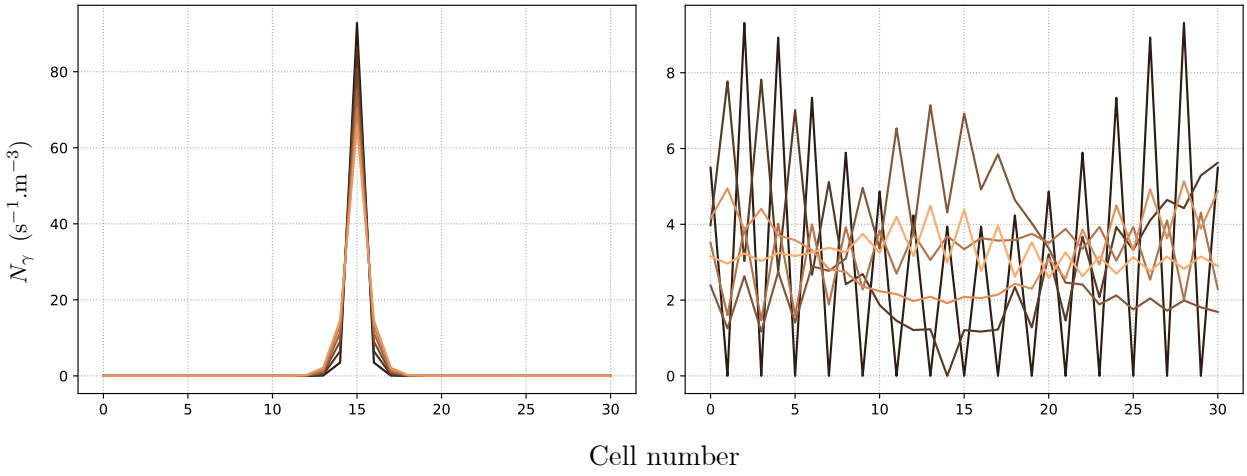

Figure 2: Comparison for different values of Cr, 0.0005 on the left and 1 on the right.

where Cr can be chosen "arbitrarily" but still needs to satisfy some conditions. Indeed, if this one is too large, information will be lost between time iteration and we get incoherent results

as shown on the right part of Figure 2. On the other hand, if Cr is too small, a large number of time iterations will happen in a given cell, drastically increasing the number of iteration to simulate the same travel distance and hence increasing the overall errors if we wanted the simulation to run over the same total distance.

In a first naive approach, we can consider the system with $c = 1\text{m.s}^{-1}$ and $\Delta x = 1\text{m}$. From the Eq.24 we can deduce an approximate value $\Delta t = 0.5\text{s}$. To start we can also take a reasonable density of photons N_γ (e.g. $N_\gamma = 100$) and consider four different cases of emission, as depicted in Figure 3.

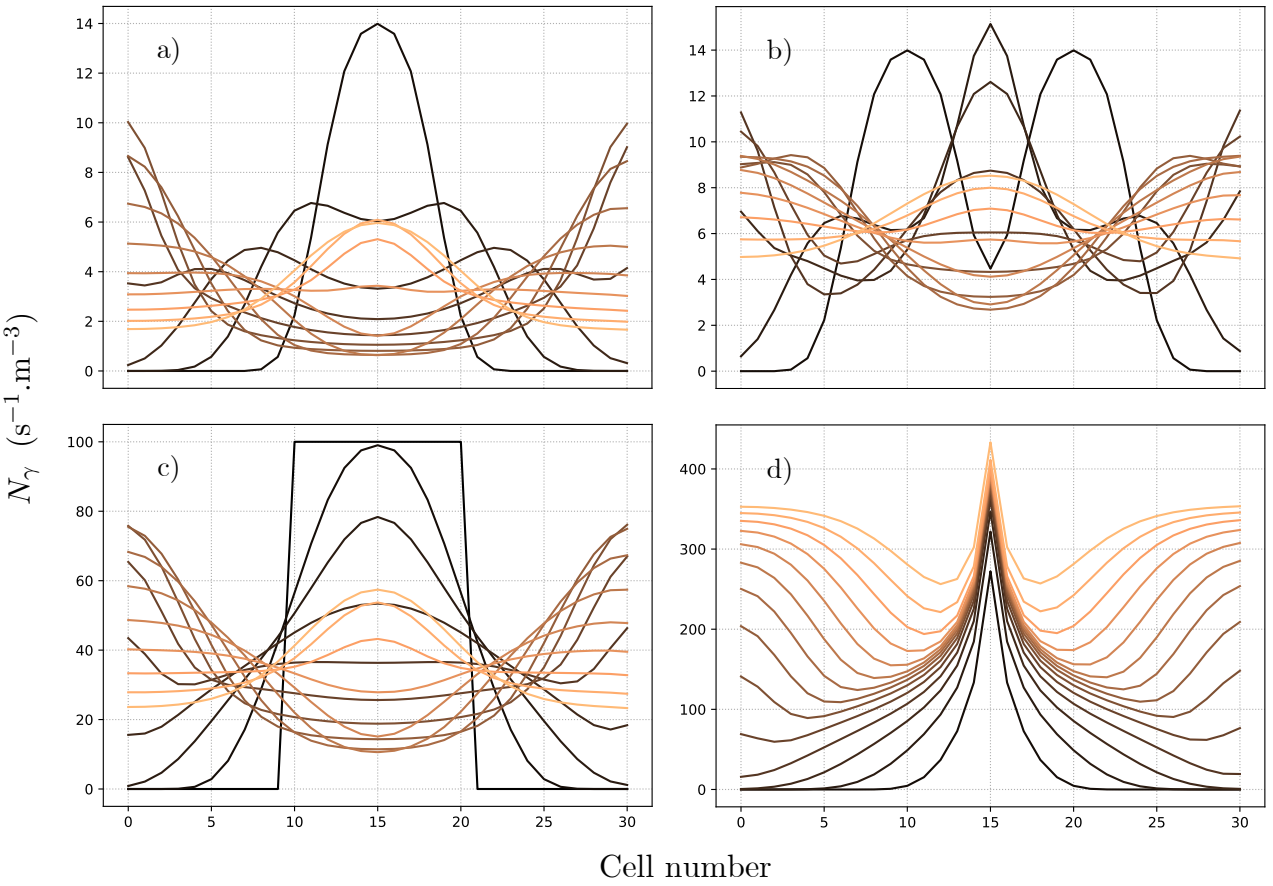

Figure 3: These four graphs are colour gradient graphs showing the time evolution of the density of photons with time over a total of 31 cells (dark = early, light = late). The four different configurations are the following. a) Single cell initial pulse. b) Double pulse. c) Pulse packet. d) Continuous single cell source.

- Single pulse source (centred): after the first time iteration, the density of photons very rapidly decreases and propagates in the neighbouring cells at a velocity which we can assume to be c (the velocity found in Eq.11). This propagation happens simultaneously in both directions around the central pulse. We can see that when these waves come into contact at the boundary (here between cell 0 and 31), they add up and go back from where they came from. This keeps happening with a general local decrease in the photon density until this one stabilises[3].

[3]We can't really see that stabilisation because the total integration time was here taken small on purpose in order to really distinguish the propagation of the pulse.

- Double pulse sources & packet pulse source: for these two sources, the general propagation and shape of the resulting densities of photons are about the same as in the case of the single pulse source.

- Continuous source: this last type of source is again similar to the three previous ones, however, contrary to the previous ones the general density of photons this time seems to increase with time. This is actually predictable, because the total number of photons introduced in the system, unlike before, is not constant.

As previously mentioned we would now like to focus a bit more on the velocity of the propagation of the wave. The best visualisation can be done using the single pulse source for which we can really see the wave fronts. In principal, those fronts should behave like a Dirac and propagate at a speed being at maximum c. Therefore what we can do is to plot as previously the time evolution of the wave, but superimposing to it the distance travelled by the speed c during a time Δt. Doing so we obtain the Figure 4 on which we can see that the wave front is actually in advance on c. This would physically be impossible because in the case in which c is the celerity of the light, it would mean that the photons would have travelled at velocities higher than c. We blame this on a numerical diffusion (due to the passage from continuous equations to discretised equations) and on the integration scheme (GLFs tend to smooth the curves that else should look like Dirac).

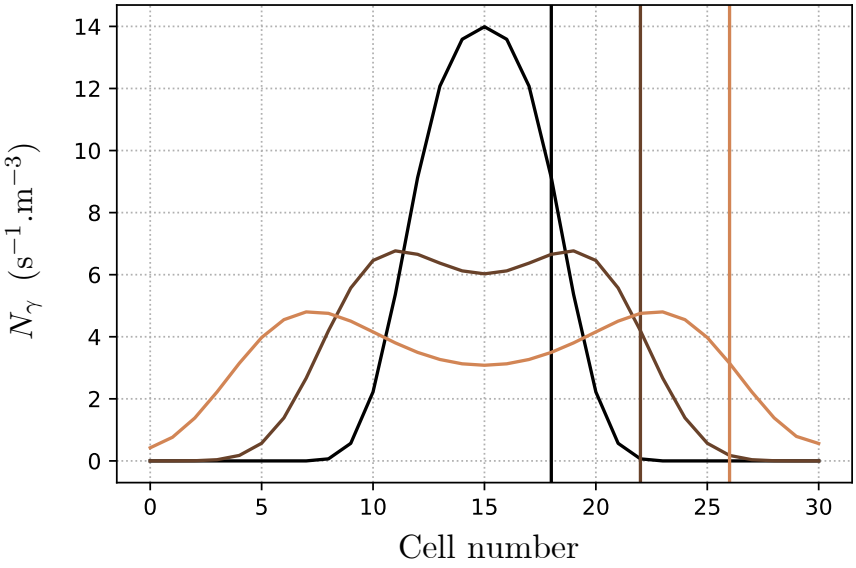

Figure 4: Time evolution of the wave front superimposed to the characteristic speed c.

3.2 Hydrogen photoionisation

Photoionisation is crucial to really be able to describe the propagation of photons in realistic cases. Hence we would like to compare this case with the previous advective solution to see if indeed the propagation is slowed down by the medium.

We introduce the photoionisation module described in Section 2.5, the results are presented in Fig.5. These four graphs show the time evolution of the number density of photons in the

case of a continuous emission. On one hand, we have the solution for the pure advection equations (black curves) and on the other hand the advection equation but this time taking into account the coupling between neutral hydrogen and photons (orange curves). As time goes by, we can observe the black curve spreading through the domain: the propagation front progresses freely in the cells as seen previously, until reaching the boundary at which point they add up. However, the curve subjected to the coupling struggles to propagate.

At the beginning of the simulation, the orange peak is much smaller than the black one. Indeed, an initial density of neutral hydrogen ρ has been initialised in all the cells of the domain with $\rho = 3$ atoms per cm^3. The source has first to ionise all the neutral hydrogen of its own cell before being able to propagate freely, this explains the "delay" between the two curve peaks (in height). Once the central cell becomes transparent, the peak can grow enough to reach the one of the black curve, as seen in graph c) and d). In addition, the front wave of the chemical solution progresses slower just as expected, due to the constant ionisations of the neutral hydrogen diminishing the flux of the incoming photons. Despite this absorption phenomena the front still successfully crosses the first cells around the source, but the effect of photoionisation can not be neglected at all as the black curve already has travelled all the domain in the same time (graph d)).

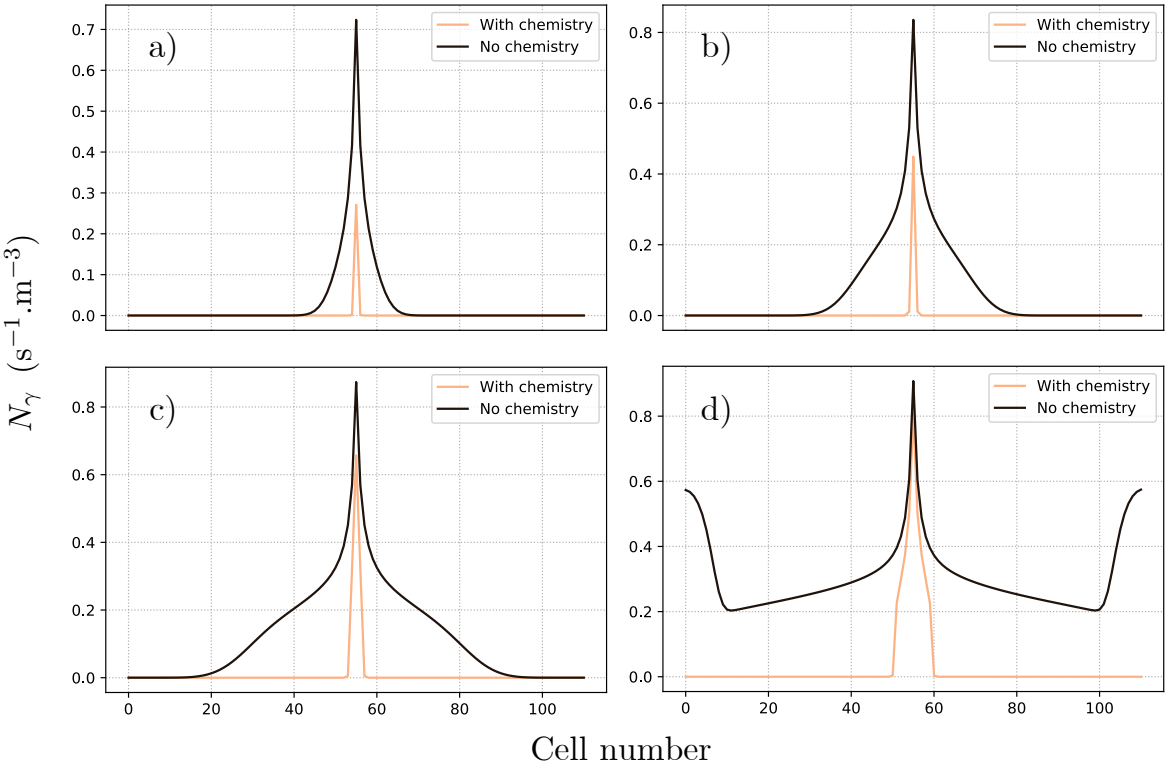

Figure 5: Evolution of the photon number density N_γ at four different time steps for the two modules of photon propagation, with graph a) the evolution of N_γ right after the start of the simulation and d) close to the end. The parameters used to plot these curves are $c = 1\text{m.s}^{-1}$, $\Delta t = 0.5\text{s}$, $\Delta x = 1\text{m}$ and $N_\gamma = 1$, on a domain of 111 cells.

We have just seen that accounting for hydrogen photoionisation had a considerable effect on the propagation of the wave front in the medium. We would now like to explore the different

regimes of that propagation, which are mainly controlled by three quantities that are the temperature, the density of hydrogen atoms, and the luminosity of the source. This time, we took realistic values for c (that is about 3×10^{10}cm.s^{-1}) and a cell size $\Delta x = 6.25$pc$= 1.93 \times 10^{19}$cm. In order to respect the current condition, we find a $\Delta t < 6.4 \times 10^8$s. We made three different types of simulation all sharing the same ground quantities: a temperature $T = 2000K$, a hydrogen atom density of $\rho = 3$ atoms per cm^3 and a photon density $N_\gamma = N\Delta t/(\Delta x)^3$ (where $N = 5 \times 10^{48}$ is the number of photons emitted by the source per second). Other parameters of the system, this time unchanged, were the total number of cells (a 111 chosen arbitrarily) and the total integration time (1×10^{12}s). We looked at the global ionisation fraction (the average ionisation in all cells) over time, only changing one parameter which resulted in Figure 6.

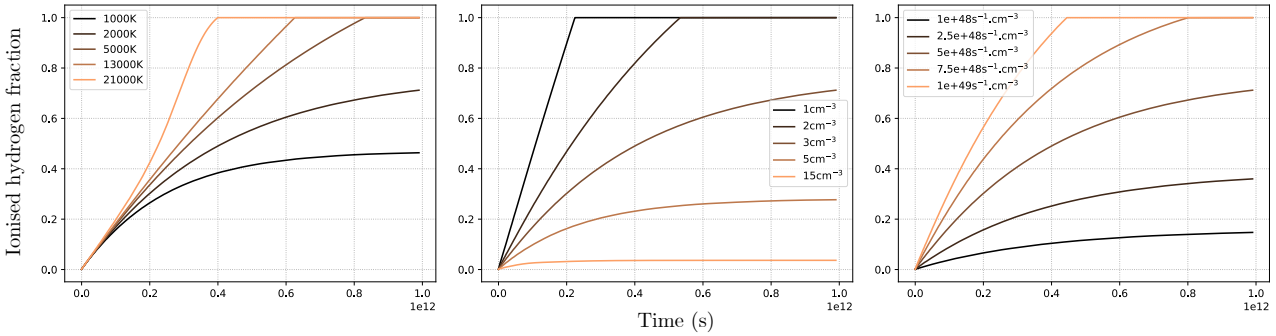

Figure 6: Each of these graphs represents the average ionised hydrogen fraction in all cells at a given time. On the left we see this evolution for five different temperatures, in the middle for five different hydrogen densities and on the right for five different photon densities.

We see that the higher the temperature, the faster the global ionisation fraction will reach one. This is due to the fact that increasing T will tend to make the collisional ionisation coefficient β to dominate over the αs recombination coefficients. Increasing the density of hydrogen atoms will diminish the effects of the photons to ionise all these atoms. Hence, for high densities (such as 15 atoms per cm^3), we see that the photons can't ionise really far from their emission source. Similarly for the photon density, the more photons there are, the easier it is for them to ionise all the atoms. In the case of our simulation we can distinguish three different regimes in Figure 6:

- The first one is the ionisation of the medium during which the wave is propagating at a given velocity, this one depending on the parameters considered.
- The second one corresponds to a medium reaching an equilibrium state after some time. By equilibrium we mean that there is a region (located around the source) which is fully ionised[4] and is surrounded by a neutral gas.
- The third regime is reached when the whole medium is ionised, in which case the photons can freely travel in our system without being perturbed by any photoionisation effects.

We can note that the distinction between the two latter ones, only has meaning in the case of a finite space because fundamentally, for finite values of the photon density, we could always increase the total size of the system an reach the equilibrium mentioned in the second point.

[4]This region of ionised medium is known as a Strömgren sphere and this notion will be further developed in section 3.3

3.3 Strömgren sphere

A Strömgren sphere is a theoretical spherical region of space surrounding a hot, luminous star and which is entirely ionised. The ionisation front, or the boundary between the fully ionised region and the partially ionised region, is materialised by the contour of the Strömgren sphere. Its volume can be determined by balancing the rate at which ionising photons are produced by the star with the rate at which they are absorbed by the surrounding gas. Other parameters such as the density of the gas or the temperature of the star also play a role in the determination of the radius of the Strömgren sphere. The 1D radius is given by:

$$L_{\text{Str}} = \frac{N_\gamma \Delta x}{\alpha_B n_H^2} \tag{25}$$

where N_γ is the photon density of the source and Δx the size of a cell in our computational domain. To observe relevant results in our simulation, we first have to compute the radius of the Strömgren sphere in order to determine the needed length for the computational domain. Therefore, it will be possible to visualise the position in the domain where the propagation front stops its advance. This will give us the numerically computed value that we will be able to compare to the theoretical one (that we now calculate).

By taking the parameters as follow: $c = 3 \times 10^{10}\text{cm.s}^{-1}$, $\Delta x = 6.25\text{pc} = 1.93 \times 10^{19}\text{cm}$, $\Delta t = 1 \times 10^{8}\text{s}$ and $N_\gamma = N\Delta t/(\Delta x)^3$ (the same ones that were used in Section 3.2), the theoretical Strömgren sphere diameter reads:

$$L_{\text{Str}} = \frac{N_\gamma \Delta x}{\alpha_B n_H^2} = 21.3 \text{ cells} \tag{26}$$

Using the same set of parameters and including the thermochemical module, we obtain the right graph of Fig.7. After an integration time of 10^{13}s, the propagation front seems to have stopped. The ionising rate is balanced with the recombination rate of the hydrogen, giving a Strömgren sphere, which diameter in the numerical simulation is of about 20 cells, therefore matching with the theoritical value previously calculated.

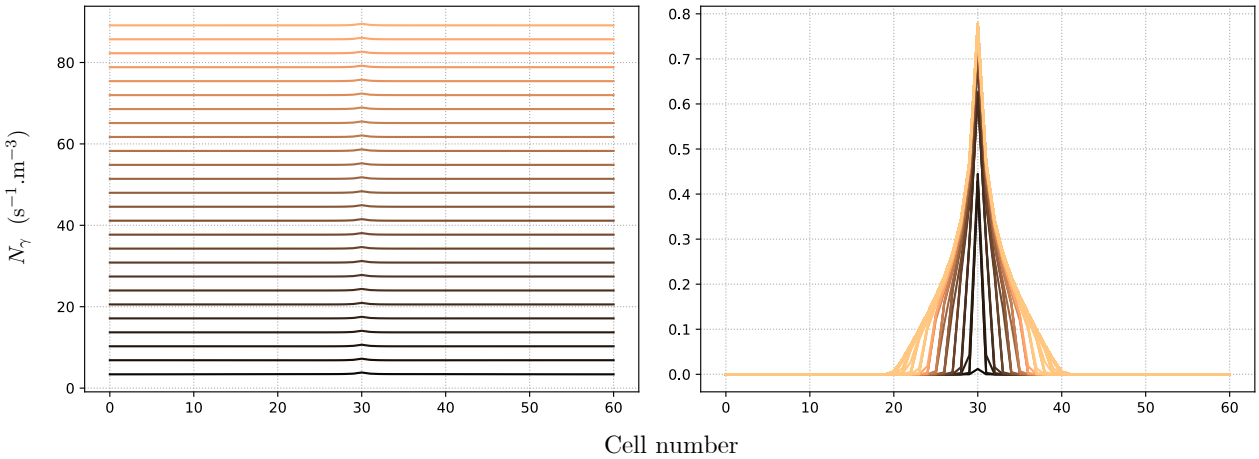

Figure 7: Both images were made with the same initial conditions, the left case does not consider any kind of thermochemical effects while the right one does. Once again we can see the coupling phenomena affecting the behaviour of the propagation.

4 Parallel computing

Code parallelisation is the process of dividing a program into smaller parts that can be executed simultaneously by different processors or cores. This can be achieved through the use of specialised libraries such as OpenMP or MPI for C-code. The main benefit of code parallelisation is increased performance and speed, as the different tasks are distributed among multiple processors. Additionally, parallelisation can also help to improve the scalability of a program, making it more efficient as the amount of data or number of cores increases.

In this code, an interesting loop to parallelise would be the main loop, that computes the numerical scheme. It can be performed by using parallel threads, by dividing the loop that iterates over the cells (second `for` loop of the function) into two smaller domains (from both sides of the domain) and assign each of these chunks to a thread. They will then compute separately the propagation of the front through the evolution of the number density of photon (N_γ), flux (F) and pressure (P) in each cells, as their computation is independent. However, it should not be forgotten to communicate the values of N_γ, F and P between the threads at the edge of each of these smaller domains. Another loop that would be interesting to parallelise is the one used for the computation of the GLFs. As their calculation only require inter-cells information, a division of the domain and assignation to different threads could also be performed. Hence, here the idea of using parallel computing could come really useful because the process is not inherently "embarrassingly parallel". Indeed as previously stated, knowing the initial values of our flux, number density and pressure at each time steps, we can independently calculate first the GLFs and then the new values.

When implementing code parallelisation into the main function which computes the numerical integration, there are several potential issues that may arise. One issue is the effects of the edges on the parallelisation process. For example, if the number of intervals cannot be divided equally among the available threads, some of them may be left with more work than others. To solve this, one solution could be to assign the few remaining bins to a single thread. Another potential problem is that the time required to gather information from different threads may overcome the benefits of parallelism. This can occur if the number of cells being processed is too small in comparison to the number of threads being used. In this case, parallelisation may not be necessary. On the other hand, if the number of cells is way greater than the number of threads, parallelism can be more efficient as each thread can run independently without having to share their boundary values very often.

5 Conclusion

In conclusion, the reionisation cosmological era is a crucial period in the history of the Universe during which the first luminous objects formed and ionised the neutral hydrogen in the Universe. Numerical simulations of radiative transfer is an essential tool in understanding this era, as it allows us to model the propagation of ionising radiation through the Universe. One of the key factors in this process is photoionisation of neutral hydrogen, which is responsible for creating the HII regions and the Strömgren spheres around the first stars. The study of these phenomena is also crucial for understanding how the first galaxies and stars formed and evolved. Overall, the reionisation era and the use of numerical simulation of radiative transfer provide a unique opportunity to understand the earliest stages of the Universe.

The approach provided in this project is one way to define the initial steps for a code describing and simulating this ionising phenomena during the reionisation epoch. It may be greatly improved and give more realistic physical results by implementing different physical effects such as the coupling of the temperature (which has been quickly discussed), a 2D or 3D implementation of the code, allowing a more detailed study of the Strömgren sphere or the consideration of the photoevaporation effect which drives through pressure the motion of hydrogen to lower pressure regions.

References

[1] D.Aubert, R.Teyssier; A radiative transfer scheme for cosmological reionization based on a local Eddington tensor. Monthly Notices of the Royal Astronomical Society, Volume 387, Issue 1, pp. 295-307. Bibcode: 2008MNRAS.387..295A

[2] Lam Hui, Nickolay Y. Gnedin, Equation of state of the photoionized intergalactic medium, Monthly Notices of the Royal Astronomical Society, Volume 292, Issue 1, November 1997, Pages 27–42

[3] C.D.Levermore; Relating Eddington factors to flux limiters. Journal of Quantitative Spectroscopy and Radiative Transfer, vol. 31, issue 2, pp. 149-160. Bibcode: 1984JQSRT..31..149L

[4] M.González, E.Audit, P.Huynh, 2007, AAP , 464, 429